Asian Journal of Chemistry; Vol. 34, No. 2 (2022), 395-401

ASIAN JOURNAL OF CHEMISTRY

https://doi.org/10.14233/ajchem.2022.23539

Photocatalytic Efficiency of Hybrid Titanium Dioxide Nanowires/Reduced Graphene Oxide (TiO_2NWs/RGO) for Degradation of Methyl Orange Dye

B.H. AZAM[1], M.A.F. MD FAUZI[1] and M.H. RAZALI[1,2,*]

[1]Faculty of Science and Marine Environment, Universiti Malaysia Terengganu, 21030 Kuala Terengganu, Terengganu, Malaysia
[2]Advanced Nanomaterials Research Group, Faculty of Science and Marine Environment, Universiti Malaysia Terengganu, 21030 Kuala Nerus, Terengganu, Malaysia

*Corresponding author: Fax: +60 9 6684660; Tel : +60 9 6683783; E-mail: mdhasmizam@umt.edu.my

Received: 18 September 2021; *Accepted*: 13 December 2021; *Published online*: 11 January 2022; AJC-20664

The aim of this research is to improve the photocatalytic efficiency by implementation of titanium dioxide nanowires/reduced graphene oxide (TiO_2NWs/RGO) hybrid photocatalyst for dye degradation. The hybrid photocatalyst TiO_2NWs/RGO was prepared using fabrication method. The physico-chemical properties of the photocatalyst was investigated by FTIR, XRD, SEM TGA, BET and their photocatalytic efficiency was evaluated for methyl orange degradation. Almost 100% of methyl orange was degraded by TiO_2NWs/RGO hybrid photocatalyst under UV light within 210 min using 1.0 g at initial concentration of methyl orange were 10 and 20 ppm. This is due to the 1D/2D heterostructures of TiO_2NWs/RGO hybrid photocatalyst that leads to the larger surface area, unique morphological and crystallinity properties, as well as excellent mobility of charge carriers and thermally stable structure

Keywords: Nanocomposites, Photocatalyst, Graphene, Degradation, Methyl orange dye.

INTRODUCTION

The textile dyeing and finishing industry has created a huge pollution problem as it is one of the most chemically intensive industries on earth and one of the main pollutants of clean water (after agriculture). Organic dyes are poisonous and damaging to human health directly or indirectly. The presence of very small amounts of dyes (< 1 mg/L for some dyes) in the water, which are nevertheless highly visible, seriously affects the aesthetic quality and transparency of water bodies such as lakes, rivers and others, leading to damage to the aquatic environment [1]. In addition, increase demand for clean water supplies has become a global issue due to rapid industrialization and population growth. As a result, a variety of practical strategies and solutions to develop more sustainable water supplies have been introduced.

Recent studies have shown that the titanium dioxide (TiO_2) materials synthesized by hydrothermal method can be used as photocatalyst to degrade a variety of organic contaminants [2,3] because of their being able to control particle size and nanostructure at low temperatures as well as being a cost-effective synthesis method accomplished of large-scale production [4,5]. Despite all the amazing properties of TiO_2 such as photostability, intrinsic electronic and surface properties, non-toxicity, cost-effectiveness and environmental friendliness [6-8], it suffers from the small surface area, large band gap which inhabits about 4% of the sunlight and cause separation possibility of photo-induced electron-hole pairs in photocatalysts is low [9]. There are many process of water treatment including traditional chemical, electrochemical and biological treatment, but this approach is limited due to low degradation performance, chemical consumption and the generation of secondary pollution [10]. To find a suitable process to remove these harmful pollutants, the photocatalysis seems to be economical and efficient approach to this issue [11]. New ways to produce more effective photocatalysts like combining semiconductors, noble metal doping and loading that recently gotten a lot of attention many researchers.

In addition, TiO_2-carbon composites can also show good photocatalytic activity under UV light [12,13]. As one of the most popular two-dimensional (2D) graphitic carbon materials, graphene possesses excellent physical and chemical properties

This is an open access journal, and articles are distributed under the terms of the Attribution 4.0 International (CC BY 4.0) License. This license lets others distribute, remix, tweak, and build upon your work, even commercially, as long as they credit the author for the original creation. You must give appropriate credit, provide a link to the license, and indicate if changes were made.

[14,15]. Graphene and graphene derivatives are being used because of their special properties of high optical transparency, high electrical conductivity, and charge transport as well as have a large surface area [16,17]. Hybrid catalysts containing graphene oxide (GO) or reduced graphene oxide (RGO) seem to have greater absorptivity [18], rapid bonding of organic molecules to the surface active sites with functional groups [19], rapid charge separation, increased photocatalytic activity, and high conductivity with a large surface area [20]. In addition, RGO shows a specific narrow band gap energy and visible light response eliminates deficiencies in degradation of dye [21,22]. RGO also was used as supports to remove the cationic impurities such as cationic dyes and heavy metal cations [23]. Therefore, in this study, nanostructured TiO_2 materials which is TiO_2 nanowires (TiO_2NWs) was synthesized and coupled with reduced graphene oxide (RGO) to produce titanium dioxide nanowires/reduced graphene oxide (TiO_2NWs/RGO) hybrid photocatalyst for degradation of methyl orange dye.

EXPERIMENTAL

All chemicals and solvents were purchased from Merck (Germany).

Synthesis of titanium dioxide nanowires (TiO_2NWs): An amount 1 g of TiO_2 was added to aqueous solution of 10 M NaOH (100 mL) and the solution was stirred with the magnetic stirrer for 30 min and the resulting suspension solution was transferred into 80 mL Teflon-lined autoclave reactor for hydrothermal treatment at 160 ºC for 10 h in the furnace. When the reaction is completed, the white precipitate obtained was washed with deionized water followed by 0.1 M HCl. The solution was filtered and washed with deionized water and ethanol respectively. Then, the white precipitate was dried at 40 ºC for 24 h in an oven. Finally, the synthesized TiO_2 was annealed at 500 ºC for 2 h.

Synthesis of reduced graphene oxide (RGO): Graphene oxide (GO) was prepared according to modified Hummer's method. In a typical synthesis, 3 g of graphite powder and 1.5 g of $NaNO_3$ was poured into 23 mL of H_2SO_4 under rapid stirring. After 30 min, 4 g of $KMnO_4$ was slowly added into mixture solution. The solution was kept under 10 ºC. The mixture solution was then transferred into 35 ± 5 ºC water bath and kept stirring for 30 min, then the mixture solution was diluted with 46 mL of deionized water and the temperature was raised up to 98 ºC. The mixture solution was diluted again with 140 mL of deionized water and left it stirred for 30 min. Finally, the mixture solution was treated with 10 mL of H_2O_2 to stop the reaction. Further, the mixture solution was washed with 5% of HCl and repeated centrifuging with deionized water. The synthesized product was dried in oven at 60 ºC overnight. Dark brown precipitate as a GO is obtained and then put into the furnace at 500 ºC for 2 h as a thermal reduction process for synthesis of reduced graphene oxide.

Fabrication of TiO_2NWs/RGO nanocomposites: The photocatalyst TiO_2NWs was dispersed in 50 mL deionized water for 30 min in ultrasonic. Next, the solution was dropwise added into 0.5 g of RGO nanosheets which dispersed in 100 mL deionized water and stirred for 10 min. The mixture solution was put in ultrasonic for 3 h. The obtained precipitate was centrifuged at 4000 rpm for 30 min and washed with deionized water several times. Finally, the solid was filtered and dried at 50 ºC for 12 h.

Characterization: FTIR spectra were conducted on Niconet 5700 FTIR spectrometer with the sample was dispersed in potassium bromide (KBr). The analysis was done from 4000-400 cm^{-1} wavenumber. The X-ray diffraction (XRD) was utilized to study the crystal structure and XRD patterns were acquired on Bruker D8 Advance X-ray diffractometer (Bruker AXS, German) at a scanning speed of 0.2º s^{-1} from 10º to 90º of 2θ. The surface morphology of catalyst was determined using scanning electron microscopy (SEM) JEOL JSM 6360LA at the operational voltage of 10 kV. Thermogravimetric analyses (TGA) was carried out using Mettler Toledo thermal analysis system TGA/DSC 1 with heating temperature over a range of 20 ºC-700 ºC to analyze the weight loss (%) and thermal stability. The N2 adsorption-desorption isotherms were recorded using Micromeritics TriStar II, at −196.2 ºC. Prior to this characterization, samples were degassed at 120 ºC for 2 h with nitrogen purging. Surface area, pore size and volume were determined using BET method. UV-Vis absorption spectra were obtained using a UV-Vis spectrophotometer (UV-2550, Shimadzu, Japan).

Photocatalytic activity: An amount of catalyst was dissolved into 100 mL of methyl orange dye solution (20 ppm). Photocatalytic degradation was carried out in dark for 30 min to attain adsorption/ desorption equilibrium between dye and photocatalyst. Next, the solution (10 mL) of initial concentration was taken out and then the solution continuously stirred was exposed to UV light. The UV light irradiation was provided by two 15 W of UV-B lamps with a fixed distance of 50 cm between samples and lamp. To define the degradation of dye, samples were filter by using 0.5 μm filter membrane after regular intervals (30 min) during the reaction. The progress of methyl orange dye degradation was monitored by considering the change in absorption peaks at 300 nm to 600 nm range in UV-Vis spectra. The photodegradation efficiency (η) was calculated using eqn. 1:

$$\text{Degradation } (\%) = \frac{A_0 - A_t}{A_0} \times 100 \quad (1)$$

where A_0 and A_t are the initial photocatalytic activity and the after photocatalytic activity various intervals of time (t), respectively.

RESULTS AND DISCUSSION

FTIR studies: The FTIR spectrum of the prepared TiO_2 NWs/RGO hybrid photocatalyst is shown in Fig 1. The presence of the water molecules on the TiO_2NWs surfaces is attributed to the existence the broad absorption around 3500-3400 cm^{-1}, which is assigned to O-H stretching vibration of the surface hydroxyl groups [24]. The observed absorption band appearing at ~1600 cm^{-1} for graphene-TiO_2 nanoparticle (GNP) and graphene-TiO_2 nanowire (GNW) indicates the skeletal vibration of the graphene sheets reduced from graphene oxide during the hydrothermal reaction [25,26]. Furthermore, the C=C stretching mode shifted slightly to higher wavelength number

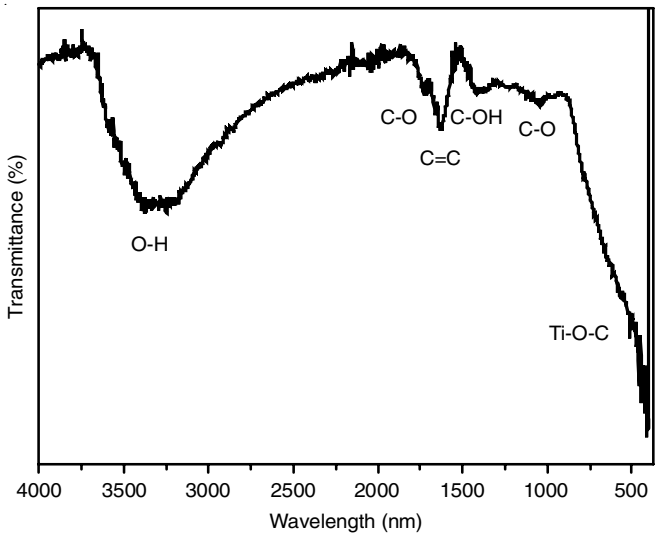

Fig. 1. FTIR spectra of TiO_2NWs/RGO hybrid

1616 cm^{-1}, probably due to the interaction of TiO_2NWs with reduced graphene oxide (RGO) [27]. Thus, complete GO reduction was accomplished since no apparent peaks could be detected, indicating that all functional groups of carbon-oxygen existed, but their characteristic peaks are only very small. The spectra broadening peak below 1000 cm^{-1} was assigned to the formation of Ti–O–C bonds (798 cm^{-1}) during the hydrothermal process overlapping with the original peak of Ti–O–Ti vibration and the existence of Ti–O–Ti bonds confirms that the chemical bonds were firmly built between graphene and TiO_2 nanostructures [28,29] as the hybrid sample representing the chemical bonding between TiO_2 and nanosheets RGO.

XRD studies: The XRD pattern of TiO_2NWs containing the peaks at 25.3º, 37.8º, 48.0º, 53.9º, 55.1º, 62.7º, 68.8º, 70.3º, and 75.0º can be indexed to (101), (004), (200), (105), (211), (204), (116), (220) and (215) tetragonal crystal planes of anatase TiO_2, as reported by other researchers [30-32]. Interestingly, no peaks assigned to rutile and brookite phase were observed even though the sample has been calcined at 500 ºC during the preparation of TiO_2NWs. In contrast, Ali *et al*. [33] reported that after calcination at 500 ºC, the presence of a mix phase of anatase and rutile TiO_2 because anatase easily transformed into rutile phase after calcination at high temperature. The formation of fully anatase TiO_2 phase structure in this study is important because it will help in increasing the photoactivity of the photocatalyst. According to Marien *et al*. [34], the anatase phase has a stronger photocatalytic property because of the higher electron mobility in the anatase crystal structure compared to rutile and brookite. However, most of the diffraction peaks in the XRD pattern of the hybrid samples can be assigned to the standard XRD pattern of tetragonal anatase TiO_2 (JCPDS No. 71-1187) indicates that the amount of RGO used has no effect on the crystalline structure of the actual products [35]. In particular, for the TiO_2NWs/RGO hybrid photocatalyst sample, peaks at 2θ of 25.3º, 37.8º, 48.0º, 53.9º, 55.1º, 62.7º, 68.8º, 70.3º and 75.0º were observed and could even be classified to (101), (004), (200), (105), (211), (204), (116), (220) and (215) crystal planes of anatase TiO_2 while (002) crystal planes of aromatic in RGO appeared at 26.2º [36]. Thus, the intensity of the TiO_2NWs peaks in anatase phase decreases after modification with RGO and pure RGO displays a broad peak that can quickly overlap with the anatase peak whenever the amount of graphene in the fabricated samples is small, inferring that a homogeneous mixture of TiO_2NWs and RGO in nanocomposite materials was obtained. The diffraction peaks of the RGO were not distinguishable in the XRD patterns of TiO_2NWs/RGO hybrid since RGO has a lower concentration and diffraction intensity than TiO_2NWs, the RGO peaks are shielded (Fig. 2) [37].

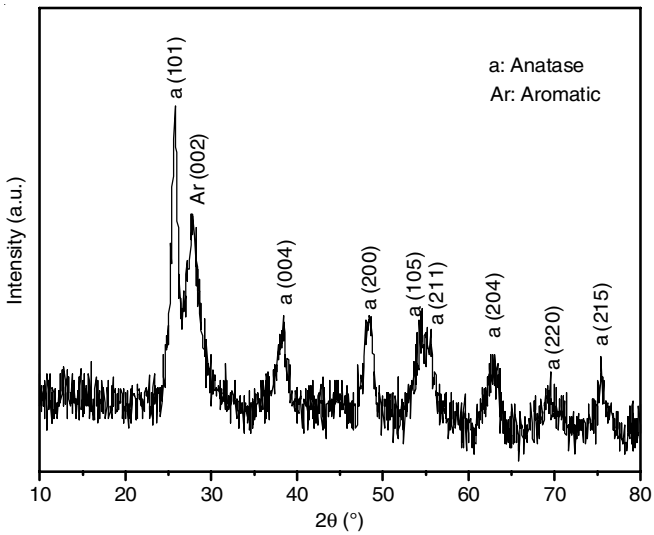

Fig. 2. XRD pattern of TiO_2NWs/RGO hybrid

SEM studies: SEM analysis was carried out to investigate the surface morphology of TiO_2NWs/RGO as shown in Fig. 3. The nanocomposite sample aggregate strongly as TiO_2NWs are enveloped by multilayer RGO in the TiO_2NWs/RGO hybrid sample. The preparation methods and mechanisms of TiO_2-based nanocomposites can explain these morphological characteristics of nanocomposites. When TiO_2 particles are treated with aqueous NaOH solution at high temperature during the hydrothermal synthesis, they change into nanosheets and assemble into nanowires on the surface of RGO [38]. The wide titanate nanosheets decomposed into very thin nanowires that cover RGO surface in a reasonable uniform fashion, although sometimes, nanowires are bundled together on RGO surface indicated by the dark colour area. Two-dimensional RGO layers prohibit TiO_2NWs from bundling, whereas one-dimensional pure TiO_2NWs prevent RGO from stacking, giving the as-prepared hybrid a large surface area [39]. It can be noticed from the SEM image that the synthesized photocatalyst nanostructures have a length of several micrometers, but the width varies from ~20 nm up to~200 nm and particular observation indicates that the larger structure is in fact nanosheets [29]. It is proposed that TiO_2NWs is easier to form a Ti–O–C bond with RGO at the locations of defects, including functional groups [40]. Next, the dye adsorption process on the surface of the composites is excellent due to the increase surface areas and acidity [41].

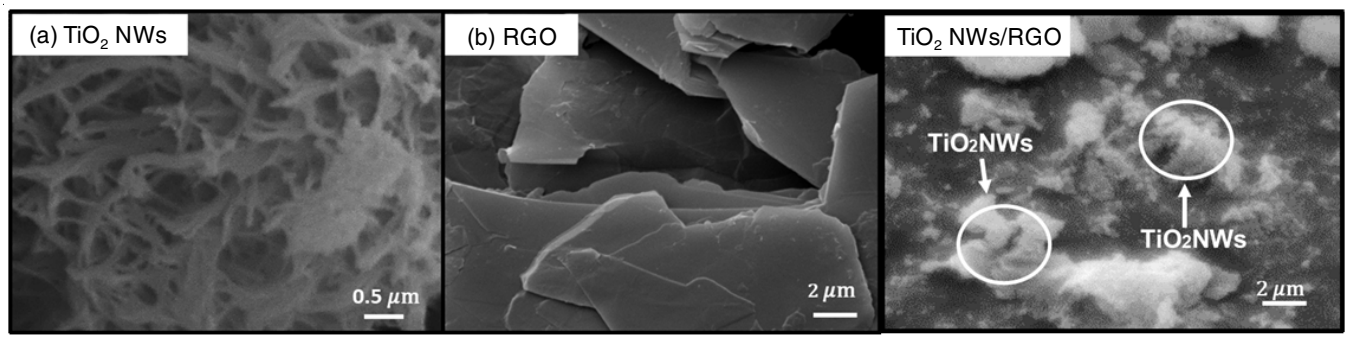

Fig. 3. SEM image for TiO_2NWs/RGO hybrid

Thermal studies: Fig. 4a shows that the weight loss of TiO_2NWs/RGO hybrid samples at the first decomposition stage 37-150 ºC is 8%, while the second decomposition stage from 150-600 ºC is also 14% weight loss. Interestingly, the last decomposition of hybrid sample is from 600 to 750 ºC with 60% weight loss, suggesting that 40% of sample is remained and thermally stable up to 900 ºC. This is probably due to the electrostatic force between RGO and TiO_2NWs in the fabricate sample as well as attributed to the availability of nitrogen environment and low oxygen groups in reduced graphene oxide that inhibit the burning and weight loss [42] as well as the presence of TiO_2NWs which assists to enhance the thermal stability of the hybrid sample and consequently, the prepared TiO_2NWs with high purity exhibit high thermal stability even at 1000 ºC [43].

N_2 absorption-desorption measurement: The specific surface area and porosity influence the efficiency of the photocatalyst. A large specific surface reabsorbs more organic molecules on the surface, which helps to reduce the recombination of photogenerated electrons and holes, improving the efficiency of the photocatalytic degradation [44]. Hence, N_2 absorption-desorption measurement was conducted to studies specific surface areas (S_{BET}) and Barret-Joyner-Halenda (BJH) pore size distribution. The S_{BET} shown that TiO_2NWs/RGO had a surface area of 102.05 m_2/g, pore size of 20 nm and pore volume of 0.49 cm^3/g. Based on previous studies by Bamba *et al.* [45], nanocomposite TiO_2/graphene (1:1) shows the S_{BET} (113 m^2/g) and total pore volume (0.243 cm^3/g) meanwhile TiO_2/graphene (2:1) sample indicate S_{BET} (52 m^2/g) and total pore volume (0.079 cm^3/g), respectively. From literature studies, it show that the different weight of graphene or TiO_2 in hybrid ratio is very essential in control the large surface area of photocatalyst that will contribute in photocatalytic activity efficiency. However, the surface area of TiO_2NWs/RGO hybrid sample is slightly lower due to the presence of agglomerated TiO_2NWs into/onto layered RGO which will block their pores but this hybrid still representing a large surface areas compared a single TiO_2NWs. The hybrid photocatalyst TiO_2NWs/RGO exhibit type IV isotherms (Fig. 4b), which indicate the presence of mesopores. The hysteresis observed in isotherms plot is matched with the H3 type characteristic for the slit shaped pores. Furthermore, the surface area can be correlated with the number of the active sites. Therefore, the larger S_{BET} TiO_2NWs/RGO indicates that this composite could be very promising in the degradation of organic pollutants [46,47].

Photocatalytic activity: The efficiency of the photocatalytic process of the different mass of TiO_2NWs/RGO was evaluated by photocatalytic degradation of methyl orange dye. The methyl orange dye absorption on the different mass of TiO_2NWs/RGO by using 100 mL of 20 ppm methyl orange dye. As shown in Fig. 5a, the TiO_2NWs/RGO dosage up to 1.5 g reduces the degradation rate of methyl orange to 87% after

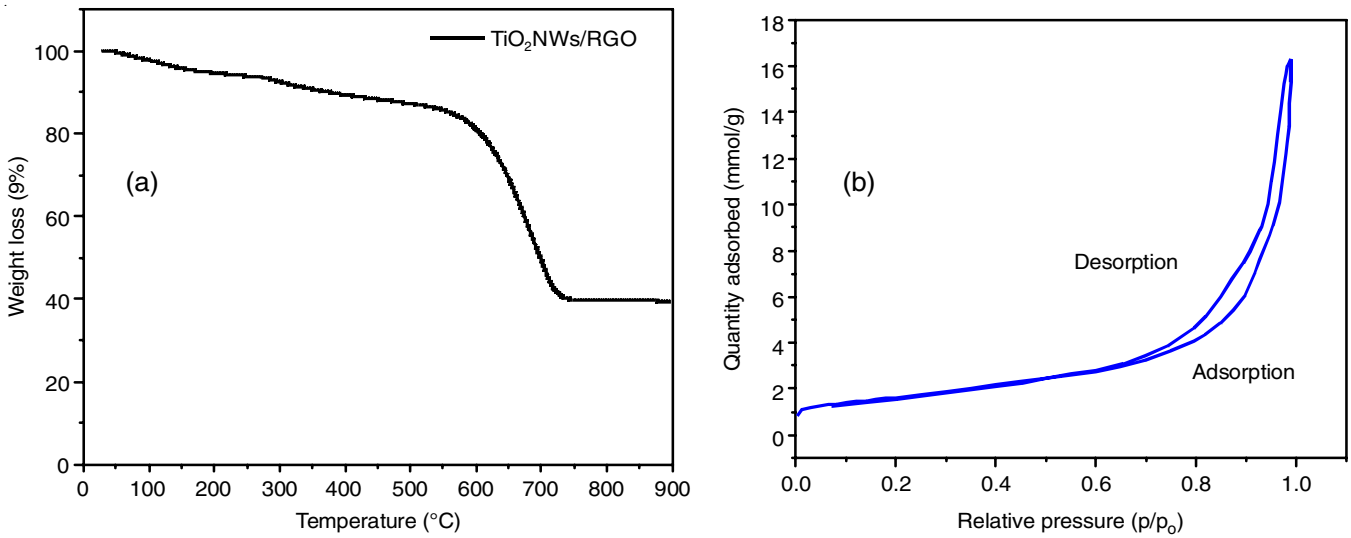

Fig. 4. (a) Thermogram and (b) N_2 adsorption-desorption isotherms of hybrid TiO_2NWs/RGO nanocomposite

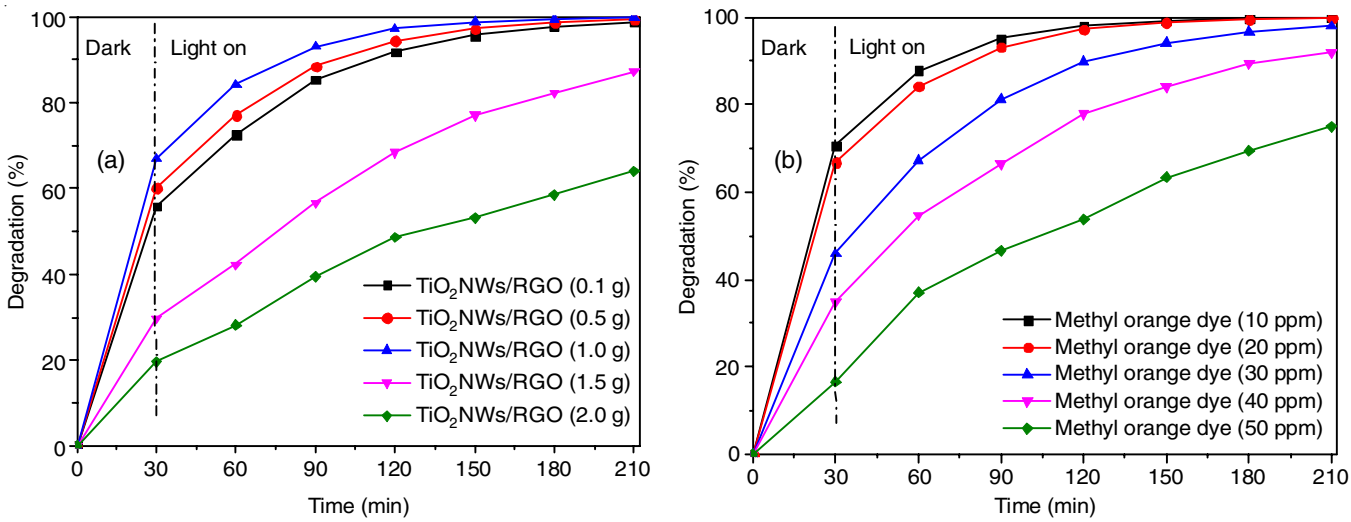

Fig. 5. (a) Photocatalytic degradation efficiency of methyl orange at different dosage of photocatalystand (b) using 1.0 g TiO_2NWs/RGO at different initial concentration methyl orange

210 min while the increment of TiO_2NWs/RGO dosage from 0.1 to 0.5 and 1.0 g was increase the degradation up to 100% after 3.5 h reaction. This is due to the presence of more active sites on TiO_2NWs/RGO hybrid photocatalyst that leading to an increments of radical hydroxyl generation to degrade methyl orange [48-50]. The photocatalysis produced oxidant reagents such as hydroxyl radicals, which can decompose contaminates, especially organic compounds. As reported by Yan *et al*. [51], the GO-TiO_2 membrane shows a photocatalytic performance only 58.8% removal rate of methylene blue dye under UV for 250 min. These results could be correlated to the enlargement of the active sites accessible to the pollutant molecules. However, Table-1 compiles the results found in the literature for methyl orange dye degradation with different photocatalysts for comparison with the TiO_2NWs/RGO hybrid catalyst presented here, which showed the better photocatalytic activity in terms of efficiency.

This is attributed to the excess amount of photocatalyst, which could leads to the hybrid photocatalyst accumulations that might serve as a boundary that hinders the passage of light to the catalyst surface [48]. Therefore, the number of accessible active centers is blocked, so depressed photocatalytic efficiency is reached. On top of that, extra dosage of photocatalyst will increase the suspension turbidity, block the light irradiation through light scattering and thus decreases the penetration of UV light during the reaction. These will decline the photocatalytic efficiency of TiO_2NWs/RGO hybrid photocatalyst for methyl orange degradation.

Fig. 5b shows the degradation of methyl orange dye using TiO_2NWs/RGO hybrid photocatalyst at different initial concentration of methyl orange. It was observed that dye removal efficiency reached up to 100% at lower concentration (10 ppm). This is because the amount of the adsorption sites on 1 g TiO_2NWs/RGO hybrid photocatalyst and $^{\bullet}OH$ radicals available were enough to adsorb the methyl orange molecules and degrade the dye *via* photocatalytic oxidation, respectively. Thus after 30 min, the removal of methyl orange was found to be more than 70% and managed to achieve 100% degradation within 180 min. Similar results was observed when initial concentration of methyl orange dye was increased up to 20 ppm even though the adsorption of methyl orange slightly lesser than 10 ppm methyl orange in first 30 min reaction. Initial concentration of 10 ppm methyl orange dye also shows slightly higher photodegradation efficiency within 90 min compared to 20 ppm but again both concentration was achieved 100% degradation after 180 min. For comparison the photocatalytic activity of synthesized TiO_2NWs/RGO hybrid nanocomposites and other photocatalyst for degradation of methyl orange dye under UV light is listed in Table-2. The TiO_2NWs/RGO hybrid nanocomposite exhibited better or comparable photocatalytic activity in methyl orange dye degradation.

However, the lack of direct contact between the methyl orange molecules and the surface of the hybrid photocatalyst due to increase mass resistance as well as less production of the active species on the TiO_2NWs surface would decrease the

TABLE-1
COMPARISON OF REPORTED PHOTOCATALYSTS EFFICIENCY USED FOR THE DEGRADATION OF METHYL ORANGE DYE

Photocatalyst	Methyl orange dye	Photodegradation efficiency	Ref.
$CoFe_2O_4$-Ag_2O (3 g)	20 ppm (200 mL)	85% after 240 min under UV light	[52]
Cu-doped ZnO (0.1 g)	20 ppm (100 mL)	88% after 240 min under UV light	[53]
TiO_2/ZnO/RGO (0.5 g)	20 ppm (1 L)	44.2% after 180 min under UV light	[54]
5% $SnSO_4$-TiO_2 (0.3 g)	20 ppm (75 mL)	91.3% after 14 h under visible light	[55]
Ag/TiO_2 (0.05 g)	7.5 ppm (100 mL)	65.4% after 120 min under UV light	[56]
TiO_2NWS/RGO (1 g)	20 ppm (100 mL)	100% after 150 min under UV light	This study

TABLE-2
RECENT REPORTS ON DIFFERENT CONCENTRATION OF METHYL ORANGE DEGRADATION

Photocatalyst	Methyl orange photodegradation	Ref.
Ag/TiO_2	35% after 120 min in 30 ppm	[56]
$C\text{-}TiO_2/RGO\text{-}WPUA$	88.3% after 6 h in 20 ppm	[57]
$RGO/Pt/3DOM\ TiO_2$	80% after 120 min in 10 ppm	[58]
$GO\text{-}TiO_2$	55% after 30 min in 20 ppm	[59]
$Ti_3C_2\text{-}TiO_2$	98% after 180 min in 30 ppm	[60]
TiO_2 nanowires	88.3% after 60 min in 10 ppm	[61]
TiO_2NWS/RGO	100% after 150 min in 20 ppm	This study

photocatalytic activity. Fig. 6 shows the reactions which take place on the surface of photocatalyst.

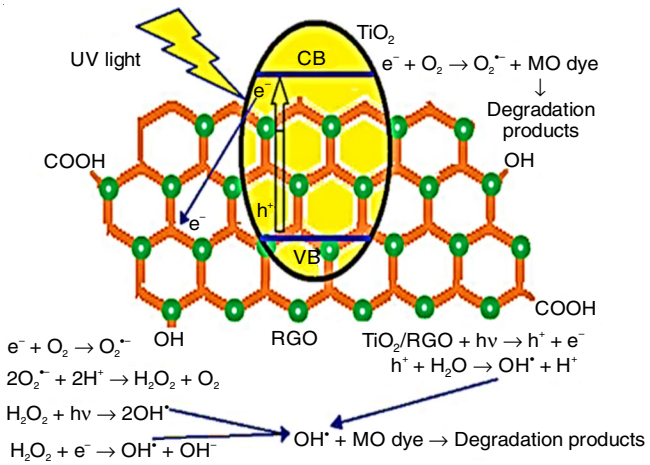

Fig. 6. Photodegradation reaction of methyl orange dye by using hybrid photocatalyst

Conclusion

The TiO_2NWs/RGO nanocomposite was fabricated method. FTIR analysis shows the presence of functional group of TiO_2NWs, RGO and XRD pattern confirmed the existence of both materials. Agglomerated TiO_2 nanowires (1D) and layered like structure (2D) of RGO were shown by SEM micrographs and XRD pattern. Hybrid has a large surface area that increase the photocatalytic activity efficiency of degradation methyl orange dye. The photocatalytic degradation of methyl orange dye was performed under different dosage of photocatalyst and different initial concentration of methyl orange dye. For different dosage of photocatalyst and different initial concentration of methyl orange dye, both reached 100% degradation within 210 min. The successful separation of photogenerated carriers and the wide optical absorption, both owing to the interaction developed between TiO_2NWs/RGO contributed to the photocatalytic efficiency capability.

ACKNOWLEDGEMENTS

The authors are grateful to Universiti Malaysia Terengganu (UMT) for facilities and Malaysia Ministry of Higher Education for the financial support vote (FRGS/1/2019/STG07/UMT/02/2).

CONFLICT OF INTEREST

The authors declare that there is no conflict of interests regarding the publication of this article.

REFERENCES

1. M.B.R. Kamalam, S. Inbanathan, K. Sethuraman, *Appl. Surf. Sci.*, **449**, 685 (2018); https://doi.org/10.1016/j.apsusc.2017.12.099
2. W. Zhao, Z. Bai, A. Ren, B. Guo and C. Wu, *Appl. Surf. Sci.*, **256**, 3493 (2010); https://doi.org/10.1016/j.apsusc.2009.12.062
3. K. Santhi, M. Navaneethan, S. Harish, S. Ponnusamy and C. Muthamizhchelvan, *Appl. Surf. Sci.*, **500**, 144058 (2019); https://doi.org/10.1016/j.apsusc.2019.144058
4. M. Asiah, M. Mamat, Z. Khusaimi, M. Achoi, S. Abdullah and M. Rusop, *Micro Eng.*, **108**, 134 (2013); https://doi.org/10.1016/j.mee.2013.02.010
5. X. Chen and S.S. Mao, *Chem. Rev.*, **107**, 2891 (2007); https://doi.org/10.1021/cr0500535
6. S.G. Kumar and L.G. Devi, *J. Phys. Chem.*, **115**, 13211 (2011); https://doi.org/10.1021/jp204364a
7. J. Schneider, M. Matsuoka, M. Takeuchi, J. Zhang, Y. Horiuchi, M. Anpo and D.W. Bahnemann, *Chem. Rev.*, **114**, 9919 (2014); https://doi.org/10.1021/cr5001892
8. M. Ni, M.K.H. Leung, D.Y.C. Leung and K. Sumathy, *Renew. Sustain. Energy Rev.*, **11**, 401 (2007); https://doi.org/10.1016/j.rser.2005.01.009
9. M. Najafi, A. Kermanpur, M.R. Rahimipour and A. Najafizadeh, *J. Alloys Compd.*, **722**, 272 (2017); https://doi.org/10.1016/j.jallcom.2017.06.001
10. M.F. Abdel-Messih, M.A. Ahmed and A.S. El-Sayed, *J. Photochem. Photobiol. Chem.*, **260**, 1 (2013); https://doi.org/10.1016/j.jphotochem.2013.03.011
11. P. Makal and D. Das, *J. Environ. Chem. Eng.*, **7**, 103358 (2019); https://doi.org/10.1016/j.jece.2019.103358
12. B. Gao, C. Peng, G. Chen and G. Lipuma, *Appl. Catal. B*, **85**, 17 (2008); https://doi.org/10.1016/j.apcatb.2008.06.027
13. B. Liu and H.C. Zeng, *Chem. Mater.*, **20**, 2711 (2008); https://doi.org/10.1021/cm800040k
14. X. Yu, W. Zhang, P. Zhang and Z. Su, *Biosens. Bioelectron.*, **89**, 72 (2017); https://doi.org/10.1016/j.bios.2016.01.081
15. X. Zhao, Y. Li, J. Wang, Z. Ouyang, J. Li, G. Wei and Z. Su, *ACS Appl. Mater. Interfaces*, **6**, 4254 (2014); https://doi.org/10.1021/am405983a
16. Z. Gao, N. Liu, D. Wu, W. Tao, F. Xu and K. Jiang, *Appl. Surf. Sci.*, **258**, 2473 (2012); https://doi.org/10.1016/j.apsusc.2011.10.075
17. X. Li, R. Shen, S. Ma, X. Chen and J. Xie, *Appl. Surf. Sci.*, **430**, 53 (2018); https://doi.org/10.1016/j.apsusc.2017.08.194
18. H. Xie, X. Ye, K. Duan, M. Xue, Y. Du, W. Ye and C. Wang, *J. Alloys Compd.*, **636**, 40 (2015); https://doi.org/10.1016/j.jallcom.2015.02.159
19. X. Wei, C. Ou, X. Guan, Z. Peng and X. Zheng, *Appl. Surf. Sci.*, **469**, 666 (2019); https://doi.org/10.1016/j.apsusc.2018.11.102
20. D. Akyuz, B. Keskin, U. Sahinturk and A. Koca, *Appl. Catal. B*, **188**, 217 (2016); https://doi.org/10.1016/j.apcatb.2016.02.003
21. B.S. Gonçalves, H.G. Palhares, T.C.D. Souza, V.G. de Castro, G.G. Silva, B.C. Silva, K. Krambrock, R.B. Soares, V.F.C. Lins, M. Houmard and E.H.M. Nunes, *J. Mater. Res. Technol.*, **8**, 6262 (2019); https://doi.org/10.1016/j.jmrt.2019.10.020
22. P. Singh , P. Shandilya, P. Raizada, A. Sudhaik, A. Rahmani-Sani and A. Hosseini-Bandegharaei, *Arab. J. Chem.*, **13**, 3498 (2020); https://doi.org/10.1016/j.arabjc.2018.12.001
23. L.K. Putri, W.J. Ong, W.S. Chang and S.P. Chai, *Appl. Mater. Today*, **4**, 9 (2016); https://doi.org/10.1016/j.apmt.2016.04.001

24. H. Fan, G. Yi, Z. Zhang, X. Zhang, P. Li, C. Zhang, L. Chen, Y. Zhang and Q. Sun, *Opt. Mater.*, **120**, 111482 (2021); https://doi.org/10.1016/j.optmat.2021.111482
25. H. Zhang, X. Lv, Y. Li, Y. Wang and J. Li, *ACS Nano*, **4**, 380 (2010); https://doi.org/10.1021/nn901221k
26. S. Wang, Y. Zhang, N. Abidi and L. Cabrales, *Langmuir*, **25**, 11078 (2009); https://doi.org/10.1021/la901402f
27. F. Bashiri, S.M. Khezri, R.R. Kalantary and B. Kakavandi, *J. Mol. Liq.*, **314**, 113 (2020); https://doi.org/10.1016/j.molliq.2020.113608
28. T. Nguyen-Phan, V.H. Pham, E.W. Shin, H.-D. Pham, S. Kim, J.S. Chung, E.J. Kim and S.H. Hur, *Chem. Eng. J.*, **170**, 226 (2011); https://doi.org/10.1016/j.cej.2011.03.060
29. X. Pan, Y. Zhao, S. Liu, C.L. Korzeniewski, S. Wang and Z. Fan, *J. Appl. Mater. Inter.*, **4**, 3944 (2012); https://doi.org/10.1021/am300772t
30. A.S. Alshammari, M.M. Halim, F.K. Yam and N.H.M. Kaus, *Mater. Sci. Semi. Proc.*, **116**, 105140 (2020); https://doi.org/10.1016/j.mssp.2020.105140
31. H. Guo, N. Jiang, H. Wang, K. Shang, N. Lu, J. Li and Y. Wu, *Appl. Catal. B*, **248**, 552 (2019); https://doi.org/10.1016/j.apcatb.2019.01.052
32. W. Sang, C. Zhan, S. Hao, L. Mei, J. Cui, Q. Zhang, X. Jin and C. Li, *J. Water Process Eng.*, **41**, 101997 (2021); https://doi.org/10.1016/j.jwpe.2021.101997
33. M.H.H. Ali, A.D. Al-Afify and M.E. Goher, *Egypt. J. Aquat. Res.*, **44**, 263 (2018); https://doi.org/10.1016/j.ejar.2018.11.009
34. C.B.D. Marien, T. Cottineau, D. Robert and P. Drogui, *Appl. Catal. B*, **194**, 1 (2016); https://doi.org/10.1016/j.apcatb.2016.04.040
35. G. Cheng, F. Xu, J. Xiong, F. Tian, J. Ding, F.J. Stadler and R. Chen, *Adv. Powder Technol.*, **27**, 1949 (2016); https://doi.org/10.1016/j.apt.2016.06.026
36. G. Nagaraju, G. Ebeling, R.V. Gonçalves, S.R. Teixeira, D.E. Weibel and J. Dupont, *J. Mol. Catal. Chem.*, **378**, 213 (2013); https://doi.org/10.1016/j.molcata.2013.06.010
37. E. Kusiak-Nejman, A. Wanag, J. Kapica-Kozar, L. Kowalczyk, M. Zgrzebnicki, B. Tryba, J. Przepiórski and A.W. Morawski, *Catal. Today*, **357**, 630 (2020); https://doi.org/10.1016/j.cattod.2019.04.078
38. N. Cao, and Y. Zhang, *J. Nanomater.*, **2015**, 168125 (2015); https://doi.org/10.1155/2015/168125
39. J. Corredor, M.J. Rivero and I. Ortiz, *Int. J. Hydrogen Energy*, **46**, 17500 (2021); https://doi.org/10.1016/j.ijhydene.2020.01.181
40. W. Zhang, Y. Tian, H. He, L. Xu, W. Li and D. Zhao, *Natl. Sci. Rev.*, **7**, 1702 (2020); https://doi.org/10.1093/nsr/nwaa021
41. W.R.K. Thalgaspitiya, T. Kankanam Kapuge, J. He, B. Deljoo, A.G. Meguerdichian, M. Aindow and S.L. Suib, *Micropor. Mesopor. Mater.*, **301**, 110521 (2020); https://doi.org/10.1016/j.micromeso.2020.110521
42. H.A. Hamad, W.A. Sadik, M.M. Abd El-latif, A.B. Kashyout and M.Y. Feteha, *J. Environ. Sci.*, **43**, 26 (2016); https://doi.org/10.1016/j.jes.2015.05.033
43. A. Mezni, *J. Mater. Res. Technol.*, **9**, 15263 (2020); https://doi.org/10.1016/j.jmrt.2020.10.104
44. J.W. Shi, J.T. Zheng and P. Wu, *J. Hazard. Mater.*, **161**, 416 (2009); https://doi.org/10.1016/j.jhazmat.2008.03.114
45. D. Bamba, M. Coulibaly, C.I. Fort, C.L. Cotet, Z. Pap, K. Vajda, E.G. Zoro, N.A. Yao, V. Danciu and D. Robert, *Phys. Status. Sol. B.*, **252**, 2503 (2015); https://doi.org/10.1002/pssb.201552219
46. Y. Chen and D.D. Dionysiou, *J. Mol. Catal. Chem.*, **244**, 73 (2006); https://doi.org/10.1016/j.molcata.2005.08.056
47. M.M. Ba-Abbad, A.A.H. Kadhum, A.B.R. Mohamad, M.S. Takriff and K. Sopian, *Int. J. Electrochem. Sci.*, **7**, 4871 (2012).
48. S.P. Deshmukh, D.P. Kale, S. Kar, S.R. Shirsath, B.A. Bhanvase, V.K. Saharan and S.H. Sonawane, *Nano-Structures Nano-Objects.*, **21**, 100407 (2020); https://doi.org/10.1016/j.nanoso.2019.100407
49. J.M. Monteagudo, A. Durán, M.R. Martínez and M.I. San, *Chem. Eng. J.*, **380**, 122410 (2019); https://doi.org/10.1016/j.cej.2019.122410
50. N.T. Padmanabhan, M.K. Jayaraj and H. John, *Catal. Today*, **348**, 63 (2019); https://doi.org/10.1016/j.cattod.2019.09.029
51. X. Yan, L. Huo, C. Ma and J. Lu, *Process Saf. Environ. Prot.*, **130**, 257 (2019); https://doi.org/10.1016/j.psep.2019.08.021
52. F. Sun, J. He, P. Wu, Q. Zeng, C. Liu and W. Jiang, *Chem. Eng. J.*, **397**, 125397 (2020); https://doi.org/10.1016/j.cej.2020.125397
53. M. Fu, Y. Li, S. Wu, P. Lu, J. Liu and F. Dong, *Appl. Surf. Sci.*, **258**, 1587 (2011); https://doi.org/10.1016/j.apsusc.2011.10.003
54. C.H. Nguyen, M.L. Tran, T.T.V. Tran and R.-S. Juang, *Sep. Purif. Technol.*, 115962 (2019); https://doi.org/10.1016/j.seppur.2019.115962
55. X. Yao, B. Zhang, S. Cui, S. Yang and X. Tang, *Appl. Surf. Sci.*, **551**, 149419 (2021); https://doi.org/10.1016/j.apsusc.2021.149419
56. X. Zheng, D. Zhang, Y. Gao, Y. Wu, Q. Liu and X. Zhu, *Inorg. Chem. Commun.*, **110**, 107589 (2019); https://doi.org/10.1016/j.inoche.2019.107589
57. G. Chen, S. Ouyang, Y. Deng, M. Chen, Y. Zhao, W. Zou and Q. Zhao, *RSC Adv.*, **9**, 18652 (2019); https://doi.org/10.1039/C9RA03250A
58. J. Huo, C. Yuan and Y. Wang, *ACS Appl. Nano Mater.*, **2**, 2713 (2019); https://doi.org/10.1021/acsanm.9b00215
59. Y. Gao, X. Pu, D. Zhang, G. Ding, X. Shao and J. Ma, *Carbon*, **50**, 4093 (2012); https://doi.org/10.1016/j.carbon.2012.04.057
60. V.Q. Hieu, T.K. Phung, T.-Q. Nguyen, A. Khan, V.D. Doan, V.A. Tran and V.T. Le, *Chemosphere*, **276**, 130154 (2021); https://doi.org/10.1016/j.chemosphere.2021.130154
61. C. Guo, J. Xu, Y. He, Y. Zhang and Y. Wang, *Appl. Surf. Sci.*, **257**, 3798 (2011); https://doi.org/10.1016/j.apsusc.2010.11.152